Marine Structures 51 (2017) 152–173

Contents lists available at ScienceDirect

Marine Structures

journal homepage: www.elsevier.com/locate/marstruc

A quasi-linear method for frictional model in helical layers of bent flexible risers

Yang Zhou [a, b], Murilo Augusto Vaz [b, *]

[a] Department of Aeronautics and Astronautics, Fudan University, Shanghai, China
[b] Ocean Engineering Program, Federal University of Rio de Janeiro, Rio de Janeiro, Brazil

ARTICLE INFO

Article history:
Received 29 March 2016
Received in revised form 18 July 2016
Accepted 10 October 2016

Keywords:
Flexible risers
Bending behaviour
Quasi-linear method

ABSTRACT

This paper deals with the behaviour of two helical layers of bent flexible risers. An analytical model with frictional effects is developed to summarize the mechanical behaviour of helical armour wires. To ensure a unified process of calculation, all formulas are simplified to build up a system of quasi-linear partial differential equations. The numerical solution is determined by finite difference method. Appropriate results are shown in the paper. The geometrical quantities, slips and stresses are matched with other analytical results and found valid.

1. Introduction

In the offshore field, unbonded flexible risers are composite structures and represent a significant part in floating production systems to provide fluid and gas transport. To adapt to the complex marine environment, flexible risers are composed of many reinforced layers which can suffer high deformation in bending behaviour, see Fig. 1. Among these layers, the tensile armour wires are one of the main parts to provide low bending stiffness relative to axial and radial stiffness and the primary cause for stress fatigue failure. Hence, the mechanical analysis of helical armour wire is the emphasis of study in bending research of flexible risers.

The bending behaviour of flexible risers, especially the research focused on tensile armour wires, has been dealt with by many authors throughout the past few decades. Different approaches have been proposed in order to search for an optimized method to predict the structural response. Féret and Bournazel [1] formulated simple equations for calculating the stresses due to that the slip of armour wires follows a geodesic direction, however no evidence has been shown to prove this axisymmetrical loads, evaluating contact pressure and relative slip between layers due to bending. It was assumedchoice. Out and von Morgen [2] considered the Euler's equation to derive the bending stress of a helical wire on a bent cylinder, and calculated the slippage of the wire also with the assumption of geodesic slip.

Witz and Tan [3] developed an analytical model for helical layers of unbonded flexible pipes. The model mainly concluded the overall resultant bending moment before and after slip using energy method. They [3] also described the hysteretic bending moment-curvature relationship. However, some important aspects including the calculation of stresses and slips still remained uncertain. Sævik [4] dealt with a 3D curved beam element by using a computational model where the curvature was prescribed, the constrained element only allowed longitudinal slip. A 2D curved finite element for umbilical analysis was

* Corresponding author.
E-mail address: murilo@oceanica.ufrj.br (M.A. Vaz).

http://dx.doi.org/10.1016/j.marstruc.2016.10.004
0951-8339/

Nomenclature

r	radius of a helical layer
R	radius of the bent pipe
θ, φ	angular coordinate
s	wire arclength
α	initial layer angle
$\boldsymbol{T}$	local unit tangential vector of the curve
$\boldsymbol{N}$	local unit normal vector of the surface
$\boldsymbol{B}$	local unit binormal vector
κ_g	geodesic curvature of the wire
κ_n	normal curvature of the wire
τ_g	torsion of the wire
$\boldsymbol{F}$,F	wire sectional force and its component in orthonormal basis
$\boldsymbol{M}$,M	wire sectional moment and its component
$\boldsymbol{p}$,	p wire distributed load and its component
m, m	wire distributed moment and its component
κ	torus curvature $1/R$
ε	relative curvature r/R
E	elastic modulus
G	shear modulus
A	wire cross sectional area
γ	tangential strain of the wire
I_N	wire second N-axial moment of area
I_B	wire second B-axial moment of area
I_P	wire second polar moment of area
Δ_T, Δ_B	wire slips in $\boldsymbol{T}$ and $\boldsymbol{B}$ directions
Δ_θ, Δ_φ	wire slips in angular coordinate directions

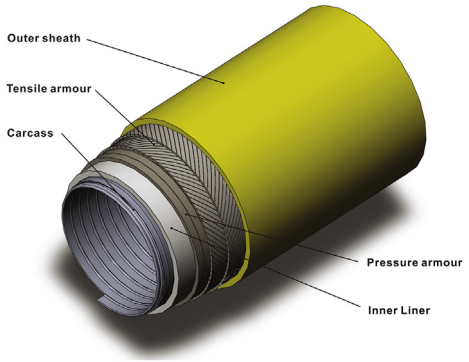

Fig. 1. The structure of flexible pipe.

also reported in Ref. [5]. Subsequently, a model included full back coupling with respect to bending stiffness by means of bi-directional shear interaction was proposed in Ref. [6]. A further development which allowed transverse slip and full 3D was reported in Refs. [7,8]. A research about theoretical and experimental studies of flexible pipes including a bending model and a 3D curved element for umbilical analysis was concluded in Ref. [9]. This work included correlation studies with respect to full scare experimental data in Ref. [4] - [6]. Costello [10] presented a model of wire ropes by applying curved beam equilibrium equations which can be a reliable reference for bending behaviour study.

Ramos and Pesce [11] developed an analytical model for analysing the structure of flexible risers associated with bending, twisting and tension. Using a system of equations including geometrical relations, constitutive equations and equilibrium conditions, all unknowns can be solved based on an assumption of full-slip of the helical layers while subjected to bending. Brack et al. [12] also studied the mechanical behaviour of flexible pipes against the potential failure modes subjected to combined axial compression, bending and torsion by using finite element method. Both theoretical and experimental results were discussed in the paper. Another finite element model was established by Bahtui et al. [13,14]. In the finite-element

model, a fully explicit time-integration scheme was used for numerical analysis. However, a few simplifying assumptions were made in the model and need to be modified in further investigation.

Féret et al. [15] investigated bending behaviour and buckling resistance of flexible armour layers. Féret and Momplot [16] established a mathematical method to calculate stresses and slips in flexible armour layers. Leroy and Estrier [17] improved the expressions of stresses and slips for both two armour layers and modeled a repeated bending behaviour with friction based on [15]. However, the system of equations were not clearly derived in detail and some assumptions were made to ensure the structure of mathematical model. Østergaard et al. [18] focused on the geometrical configuration which exactly satisfies the equations of equilibrium for a curved beam on a frictionless toroid, then in Ref. [19], Østergaard et al. considered frictional forces and developed the model under compression and bending configuration. Moreover, Tension behaviour and Buckling collapse study of flexible pipes were also investigated by both analytical model and laboratory test in Refs. [20,21]. Tang et al. [22] summarized seven analytical models available in literature that basically covered the majority of the bending behaviour research, and developed a three-dimensional finite element model for investigation.

Among these papers, due to peculiar method and complicated system of equations, Leroy and Estrier's model [17] has become a meaningful topic to follow. Meanwhile, there still have some unclear parts in the paper including geometrical model and numerical solution. The research presented in this paper discusses the bending behaviour of two helical layers with friction. The mechanics of the frictional model in helical layers of bent flexible risers is based on Leroy and Estrier's model [17]. Note that, one armour wire in each layer will be studied due to identical characteristics of each individual helical wire.

The method proposed in the paper aims to determine a unified numerical implementation which is a totally mathematical analysis for this bending problem, all equations are clearly and detailedly demonstrated to show the principle of flexible pipe's mathematical model compared to Leroy and Estrier [17]. Moreover, the final numerical solution in Ref. [17] was determined with a non-linear method, which is hard to ensure the accuracy and efficiency of results while applying to various data. Many nonlinear numerical solution cannot guarantee the stability and blindly performs arithmetic on numbers without actually examining the case and data first. In the present paper, simplicity of the algorithms has been emphasized, all formulas are therefore simplified in moderation in order to build up a system of quasi-linear partial differential equations. Compared to nonlinear method, quasi-linear method can efficiently reduce calculation time while the numbers of data increase significantly. The good agreement found from analytical comparisons verifies accuracy of the proposed method. The quasi-linear implementation will be put forward as follows.

2. Theory

The model theory for helical layers of bent flexible risers is divided into three parts. Firstly, the geometrical analysis of a torus surface is illustrated. The helical wires are deformed with the variation of bending curvature, nevertheless, the accurate deformation is unknown. Secondly, mechanical analysis, including equilibrium equations and constitutive relations are presented based on the local orthogonal vectors frame. The third part is the discussion of friction model, which is clear to demonstrate the pipes' behaviour by using the slips of two orthogonal directions.

2.1. Geometrical equations

To investigate the structure behaviour of helical wires embedded on a torus, a parameterization of a bent torus surface must be established. In order to define the location of a point on surface, allowing for a conceptual simplification of moving frames, two parameters θ and φ are chosen to determine this surface as a mathematical model, see Fig. 2. The torus equations by Cartesian coordinates in matrix form is.

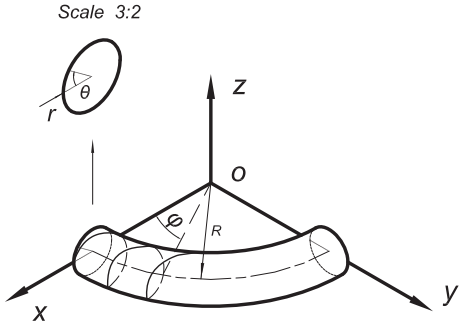

Fig. 2. Mathematical model.

$$\boldsymbol{\Sigma}(\theta,\varphi)=\begin{bmatrix}x(\theta,\varphi)\\ y(\theta,\varphi)\\ z(\theta,\varphi)\end{bmatrix}=\begin{bmatrix}(R+r\cdot\cos\theta)\cos\varphi\\ (R+r\cdot\cos\theta)\sin\varphi\\ r\cdot\sin\theta\end{bmatrix} \tag{1}$$

Where, r is the radius of a helical layer, R is the radius of the bent pipe. Each point, following a Cartesian description on the torus surface, is now valid and given by Eq. (1) if two parameters θ and φ are determined, and this surface is continuous and smooth, namely, all the geometrical quantities can be deduced from (1), including three local unit vectors ($\boldsymbol{T}$,$\boldsymbol{N}$,$\boldsymbol{B}$) of an arbitrary curve adhering to this surface and the relation between arc length s and parameter θ. For this case, a curve on a surface, the normal vector of surface $\boldsymbol{N}$ is determined instead of the normal vector of curve $\boldsymbol{n}$. Moreover, the tangential vectors are coincident. Hence, there will be a rotation from Frenet-Serret frame ($\boldsymbol{t}$,$\boldsymbol{n}$,$\boldsymbol{b}$) to Darboux frame ($\boldsymbol{T}$,$\boldsymbol{N}$,$\boldsymbol{B}$), see Fig. 3. All the following details and derivation of geometrical quantities will be based on the theory of differential geometry by do Carmo's textbook [23].

The unit normal vector $\boldsymbol{N}$ can be derived by the surface derivatives with respect to torus coordinates, which span the tangent space of torus surface.

$$\boldsymbol{N}=\frac{\frac{\partial\boldsymbol{\Sigma}}{\partial\theta}\times\frac{\partial\boldsymbol{\Sigma}}{\partial\varphi}}{\left|\frac{\partial\boldsymbol{\Sigma}}{\partial\theta}\times\frac{\partial\boldsymbol{\Sigma}}{\partial\varphi}\right|}=\frac{\boldsymbol{\Sigma}\theta\times\boldsymbol{\Sigma}_{\varphi}}{\left|\boldsymbol{\Sigma}\theta\times\boldsymbol{\Sigma}_{\varphi}\right|}=\begin{bmatrix}-\cos\theta\cos\varphi\\ -\cos\theta\sin\varphi\\ -\sin\theta\end{bmatrix} \tag{2}$$

The unit tangential vector $\boldsymbol{T}$ can not be given on explicit form. However, assuming α is the initial layer angle of helix from the unit tangential vector of coordinates φ defined as $\boldsymbol{t}_{\varphi}$ to unit tangential vector $\boldsymbol{T}$, and if angle α is confirmed, one wire curve will be fixed, θ and φ will hold a specific relation, the unit tangential vector $\boldsymbol{T}$ can be derived as follows.

Let θ be the only parameter of the curve, considering the arc length s by definition is

$$s(\theta)=\int_{\theta_0}^{\theta}\left|\frac{\mathrm{d}\boldsymbol{\Sigma}(\theta)}{\mathrm{d}\theta}\right|\mathrm{d}\theta \tag{3}$$

Then the unit tangential vector $\boldsymbol{T}$ will be given by

$$\boldsymbol{T}=\frac{\frac{\mathrm{d}\boldsymbol{\Sigma}(\theta)}{\mathrm{d}\theta}}{\left|\frac{\mathrm{d}\boldsymbol{\Sigma}(\theta)}{\mathrm{d}\theta}\right|}=\frac{\mathrm{d}\boldsymbol{\Sigma}(\theta)}{\mathrm{d}\theta}\cdot\frac{\mathrm{d}\theta}{\mathrm{d}s}$$

$$=\begin{bmatrix}-(R+r\cdot\cos\theta)\sin\varphi\dfrac{\mathrm{d}\varphi}{\mathrm{d}\theta}-r\cdot\sin\theta\cos\varphi\\ (R+r\cdot\cos\theta)\cos\varphi\dfrac{\mathrm{d}\varphi}{\mathrm{d}\theta}-r\cdot\sin\theta\sin\varphi\\ -r\cdot\cos\theta\end{bmatrix}\cdot\frac{\mathrm{d}\theta}{\mathrm{d}s} \tag{4}$$

The relation between arc length s and coordinate θ can be derived from Eqs. (3)–(1)

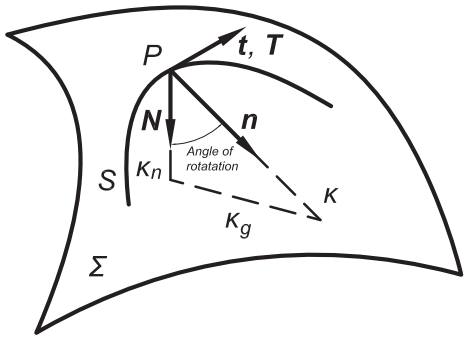

Fig. 3. Local frame transformation.

$$\left(\frac{\mathrm{d}s}{\mathrm{d}\theta}\right)^2 = \left(\left|\frac{\mathrm{d}\boldsymbol{\Sigma}(\theta)}{\mathrm{d}\theta}\right|\right)^2 = \sqrt{\left(\frac{\mathrm{d}x}{\mathrm{d}\theta}\right)^2 + \left(\frac{\mathrm{d}y}{\mathrm{d}\theta}\right)^2 + \left(\frac{\mathrm{d}z}{\mathrm{d}\theta}\right)^2} = r^2 + (R + r\cdot\cos\theta)^2\left(\frac{\mathrm{d}\varphi}{\mathrm{d}\theta}\right)^2 \tag{5}$$

Meanwhile the unit binormal vector $\boldsymbol{B}$ can be calculated by

$$\boldsymbol{B} = \boldsymbol{T} \times \boldsymbol{N} \tag{6}$$

Hence, in order to calculate the three local unit vectors ($\boldsymbol{T}$,$\boldsymbol{N}$,$\boldsymbol{B}$), the key point is to determine the relation between torus coordinates θ and φ. Leroy and Estrier [17] suggested the following assumption

$$\begin{cases} \dfrac{\mathrm{d}\varphi}{\mathrm{d}\theta} = \dfrac{\varepsilon}{\tan\alpha}(1 + h(\theta,\varepsilon)) \\ h(\theta,\varepsilon) = -\dfrac{1}{r\cdot\cos\alpha}\cdot\dfrac{\mathrm{d}\Delta_B}{\mathrm{d}\theta} \end{cases} \tag{7}$$

Where ε=r/R is the relative bending curvature, Δ_B denotes the wire slip in $\boldsymbol{B}$ direction, and α represents the initial layer angle of helix which is assumed as a constant in the equation. Eq. (7) was developed by Leroy and Estrier [17] and this assumption is the only approximation in geometrical part.

All the geometrical quantities presented above are the intrinsic features of surface and will as initial data contribute to the next analysis of mechanical parts.

2.2. Equilibrium equations

In order to study the mechanical behaviour of helical wires on torus, the direct approach is to establish a system of equilibrium equations. According to the nature of armour wires, the kinematic description of local orthogonal vectors frame must be determined so that the equilibrium equations will transform from a vectorial form to a componentwise form.

The differential formula of moving Darboux frame ($\boldsymbol{T}$,$\boldsymbol{N}$,$\boldsymbol{B}$) with respect to arc length s is defined as

$$\mathrm{d}\begin{bmatrix}\boldsymbol{T}\\ \boldsymbol{N}\\ \boldsymbol{B}\end{bmatrix} = \begin{bmatrix}0 & \kappa_n\mathrm{d}s & \kappa_g\mathrm{d}s\\ -\kappa_n\mathrm{d}s & 0 & -\tau_g\mathrm{d}s\\ -\kappa_g\mathrm{d}s & \tau_g\mathrm{d}s & 0\end{bmatrix}\begin{bmatrix}\boldsymbol{T}\\ \boldsymbol{N}\\ \boldsymbol{B}\end{bmatrix} \tag{8}$$

Where κ_g is the geodesic curvature, κ_n is normal curvature and τ_g is torsion of the wire. Note that, in differential geometry, the sign of κ_g depends on the orientations of the surface and curve. In current model, a positive geodesic curvature is defined by the fact that the arc length s and coordinates θ, φ change at a same orientation. That means s and θ, φ should increase both positive or negative. The geodesic curvature κ_g changes sign when the orientation of either surface or curve is changed.

On basis of Eq. (8) with three local unit vectors' expressions in Eqs. (2), (4) and (6), κ_g, κ_n and τ_g can be derived by

$$\begin{aligned} \kappa_g &= -\boldsymbol{T}\cdot\frac{\mathrm{d}\boldsymbol{B}}{\mathrm{d}s} = \boldsymbol{B}\cdot\frac{\mathrm{d}\boldsymbol{T}}{\mathrm{d}s} \\ \kappa_n &= \boldsymbol{N}\cdot\frac{\mathrm{d}\boldsymbol{T}}{\mathrm{d}s} = -\boldsymbol{T}\cdot\frac{\mathrm{d}\boldsymbol{N}}{\mathrm{d}s} \\ \tau_g &= -\boldsymbol{B}\cdot\frac{\mathrm{d}\boldsymbol{N}}{\mathrm{d}s} = \boldsymbol{N}\cdot\frac{\mathrm{d}\boldsymbol{B}}{\mathrm{d}s} \end{aligned} \tag{9}$$

The final expressions of κ_g, κ_n and τ_g derived by Eq. (9) are

$$\kappa_g = \left\{\sin\theta\left[2r^2\left(\frac{\mathrm{d}\varphi}{\mathrm{d}\theta}\right) + R^2(1+\varepsilon\cos\theta)^2\left(\frac{\mathrm{d}\varphi}{\mathrm{d}\theta}\right)^3\right] - rR(1+\varepsilon\cos\theta)\left(\frac{\mathrm{d}^2\varphi}{\mathrm{d}\theta^2}\right)\right\}\left(\frac{\mathrm{d}\theta}{\mathrm{d}s}\right)^3 \tag{10}$$

$$\kappa_n = \left[r + R(1+\varepsilon\cos\theta)\cos\theta\left(\frac{\mathrm{d}\varphi}{\mathrm{d}\theta}\right)^2\right]\left(\frac{\mathrm{d}\theta}{\mathrm{d}s}\right)^2 \tag{11}$$

$$\tau_g = R\left(\frac{\mathrm{d}\varphi}{\mathrm{d}\theta}\right)\left(\frac{\mathrm{d}\theta}{\mathrm{d}s}\right)^2 \tag{12}$$

Substituting Eq. (8) into the following equilibrium equations for a curved beam on vectorial form which are widely used in mechanical analysis of curved beam by many authors like Reissner [24], Ericksen and Truesdell [25],

$$\begin{aligned} \frac{\mathrm{d}\boldsymbol{F}}{\mathrm{d}s} + \boldsymbol{p} &= 0 \\ \frac{\mathrm{d}\boldsymbol{M}}{\mathrm{d}s} + \boldsymbol{T}\times\boldsymbol{F} + \boldsymbol{m} &= 0 \end{aligned} \tag{13}$$

the componentwise equations of equilibrium are developed by

$$\begin{aligned} \frac{\mathrm{d}F_T}{\mathrm{d}s} - \kappa_n F_N - \kappa_g F_B + p_T &= 0 \\ \frac{\mathrm{d}F_N}{\mathrm{d}s} + \kappa_n F_T + \tau_g F_B + p_N &= 0 \\ \frac{\mathrm{d}F_B}{\mathrm{d}s} + \kappa_g F_T - \tau_g F_N + p_B &= 0 \\ \frac{\mathrm{d}M_T}{\mathrm{d}s} - \kappa_n M_N - \kappa_g M_B + m_T &= 0 \\ \frac{\mathrm{d}M_N}{\mathrm{d}s} + \kappa_n M_T + \tau_g M_B - F_B + m_N &= 0 \\ \frac{\mathrm{d}M_B}{\mathrm{d}s} + \kappa_g M_T - \tau_g M_N + F_N + m_B &= 0 \end{aligned} \tag{14}$$

In Eq. (13), $\boldsymbol{F}$ and $\boldsymbol{M}$ represent sectional forces and moments on vectorial forms, $\boldsymbol{p}$ and $\boldsymbol{m}$ are assumed to be integrable functions of arc length s, denote the assigned force and moment per unit length. While in Eq. (14), F_T, F_N, F_B and M_T, M_N, M_B represent the component sectional forces and moments along directions of $\boldsymbol{T}$, $\boldsymbol{N}$, $\boldsymbol{B}$ respectively. p_T, p_N, p_B and m_T, m_N, m_B respectively represent the component distributed forces and moments corresponding to $\boldsymbol{p}$ and $\boldsymbol{m}$. These mechanical quantities will be derived by the later constitutive relations. Derivation of equilibrium equations are based on Love's terminal textbook [26].

2.3. Constitutive relations

The following constitutive relations are routinely used so as to combine forces and deformations:

$$\begin{aligned} F_T &= EA\gamma \\ M_B &= EI_B\Delta\kappa_n \\ M_N &= -EI_N\Delta\kappa_g \\ M_T &= -GI_\rho\Delta\tau_g \end{aligned} \tag{15}$$

Where, E and G respectively represent elastic and shear moduli, A is cross sectional area of the wire, and I_N, I_B, I_P are the wire second moment of area. These quantities are known as constants when in practical analysis. γ is the tangential strain. It has the following linear simplified form with respect to Δ_T, which denotes the wire slip in $\boldsymbol{T}$ direction by Leroy and Estrier's derivation [17].

$$\gamma = \frac{\sin\alpha}{r}\frac{\mathrm{d}\Delta_T}{\mathrm{d}\theta} + \varepsilon\cos^2\alpha\cos\theta \tag{16}$$

It is noted that here the tangential force F_T is only caused by pure bending, not including the initial tangential forces on both ends corresponding to practical application.

$\Delta\kappa_n$, $\Delta\kappa_g$, $\Delta\tau_g$ are the changes of curvatures corresponding to the bent pipe which are given by the following expressions, respectively

$$\begin{aligned}\Delta\kappa_g &= \kappa_g - \kappa_g^{ini}\\ \Delta\kappa_n &= \kappa_n - \kappa_n^{ini}\\ \Delta\tau_g &= \tau_g - \tau_g^{ini}\end{aligned} \tag{17}$$

Where, κ_g^{ini}, κ_n^{ini} and τ_g^{ini} represent the initial curvature components of the armour wire when the pipe's curvature is zero, i.e. ε=0.

However, the final expressions of $\Delta\kappa_g$, $\Delta\kappa_n$ and $\Delta\tau_g$ are complex and difficult for analytical analysis by solving Eqs. (10)–(12). Applying Eq. (7), the following process is to linearize the expression of $\Delta\kappa_g$, $\Delta\kappa_n$ and $\Delta\tau_g$.

κ_g, κ_n and τ_g change with respect to bending curvature of torus. Considering the initial helical state that the structure is unloaded, torus is right cylinder while armour wires are perfect helixes, then

$$\begin{cases} \dfrac{r}{R} = \varepsilon = 0\\ h(\theta, \varepsilon = 0) = 0\\ \dfrac{\mathrm{d}^2\varphi}{\mathrm{d}\theta^2} = 0 \end{cases} \tag{18}$$

By substituting Eq. (18) into Eqs. (10)–(12), the initial curvatures κ_g^{ini}, κ_n^{ini} and τ_g^{ini} can be given by

$$\begin{aligned}\kappa_g^{ini} &= \sin\theta\left(2r^2\cdot\frac{\varepsilon}{\tan\alpha} + R^2\cdot\frac{\varepsilon^3}{\tan^3\alpha}\right)\frac{\sin^2\alpha}{r^2} = 0\\ \kappa_n^{ini} &= \left(r + R\cdot\cos\theta\cdot\frac{\varepsilon^2}{\tan^2\alpha}\right)\frac{\sin^2\alpha}{r^2} = \frac{\sin^2\alpha}{r}\\ \tau_g^{ini} &= R\cdot\frac{\varepsilon}{\tan\alpha}\cdot\frac{\sin^2\alpha}{r^2} = \frac{\cos\alpha\sin\alpha}{r}\end{aligned} \tag{19}$$

When bending curvature of torus is no longer null, by substituting the full expression of Eq. (7) into Eqs. (10)–(12), meanwhile, using the following simplified Eq. (5) to replace the relation between arc length s and coordinate θ,

$$\begin{aligned}\left(\frac{\mathrm{d}s}{\mathrm{d}\theta}\right)^2 &= r^2 + (R + r\cdot\cos\theta)^2\left(\frac{\mathrm{d}\varphi}{\mathrm{d}\theta}\right)^2\\ &\approx r^2 + R^2\cdot\frac{\varepsilon^2}{\tan^2\alpha} = \left(\frac{r}{\sin\alpha}\right)^2\end{aligned} \tag{20}$$

from Eqs. (10)–(12), the changes of κ_g, κ_n and τ_g can be simplified into linear forms

$$\Delta\kappa_g = \frac{\varepsilon}{r}\cos\alpha\left(1 + \sin^2\alpha\right)\sin\theta + \frac{\sin^2\alpha}{r^2}\cdot\frac{\mathrm{d}^2\Delta_B}{\mathrm{d}\theta^2} \tag{21}$$

$$\Delta\kappa_n = \frac{\varepsilon}{r}\cos^2\alpha\left[\left(1 - 2\sin^2\alpha\right)\cos\theta - 2\frac{h}{\varepsilon}\sin^2\alpha\right] \tag{22}$$

$$\Delta\tau_g = \frac{\varepsilon}{r}\cos\alpha\sin\alpha\left[-2\cos^2\alpha\cos\theta + \left(\sin^2\alpha - \cos^2\alpha\right)\frac{h}{\varepsilon}\right] \tag{23}$$

Eq. (21)–(23) were presented by Leroy and Estrier [17]. The formulas of $\Delta\kappa_g$, $\Delta\kappa_n$ and $\Delta\tau_g$ are simplified into linear forms in order to validate the process of analytical calculation. The derivation of simplification is clearly included here in order to ensure the accuracy of calculation. Moreover, Eqs. (16) and (21) to (23) combine tangential strain and geometrical quantities with wire slips Δ_B and Δ_T which will be convenient for frictional analysis.

2.4. Analysis of friction

When helical wires begin to slip, the local frame moves. Then the trace will generate two kinds of orthogonal direction slips (Δ_B,Δ_T) and (Δ_θ,Δ_φ), see Fig. 4. Δ_B and Δ_T are the wire slips along binormal direction $\boldsymbol{B}$ and tangential direction $\boldsymbol{T}$, while Δ_θ and Δ_φ represent the wire slips along the unit tangential directions of two coordinates θ and φ, respectively.

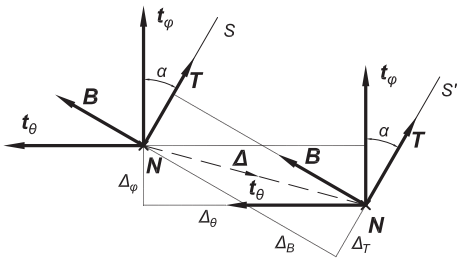

Fig. 4. Local frame transformation.

From Fig. 4, the relation between two orthogonal direction slips (Δ_B,Δ_T) and (Δ_θ,Δ_φ) is the following expression

$$\begin{bmatrix}\Delta_\theta\\ \Delta_\varphi\end{bmatrix}=\begin{bmatrix}\cos\alpha & \sin\alpha\\ -\sin\alpha & \cos\alpha\end{bmatrix}\begin{bmatrix}\Delta_B\\ \Delta_T\end{bmatrix} \tag{24}$$

In the analysis of friction (Δ_B,Δ_T), are chosen as the armour wires' displacements to develop frictional model, note that all equations above are appropriate for both two armour layers, whereas the formulas in armour layers 1 and 2 will be shown in different expressions while considering friction effects.

Since α is the initial layer angle which is considered as a constant, the subscripts 1 and 2 refer to the i th layer (i=1,2), $\overline{\alpha}$ is given to hold a simpler form in frictional model:

$$\overline{\alpha}=\alpha_2-\alpha_1 \tag{25}$$

The relative slip of layer 2 which is defined as δ^2 will hold a relationship with the slip of layer 1 in the following matrix form

$$\begin{bmatrix}\delta_B^2\\ \delta_T^2\end{bmatrix}=\begin{bmatrix}\Delta_B^2\\ \Delta_T^2\end{bmatrix}-\begin{bmatrix}\cos\overline{\alpha} & -\sin\overline{\alpha}\\ \sin\overline{\alpha} & \cos\overline{\alpha}\end{bmatrix}\begin{bmatrix}\Delta_B^1\\ \Delta_T^1\end{bmatrix} \tag{26}$$

(Δ_B,Δ_T) and (δ_B,δ_T) can point out the slip directions of two layers of armour wires. In addition, the component frictional forces along directions $\boldsymbol{T}$ and $\boldsymbol{B}$ must be determined while calculated in Eq. (14), the following scalar components $q_{f,T}$ and $q_{f,B}$ (per unit length of a helix) are the orthogonal projections of friction force onto the two unit vectors in the directions of $\boldsymbol{T}$ and $\boldsymbol{B}$ respectively.

For layer 1:

$$\begin{aligned}q_{f,B}^1&=-\frac{\dot{\Delta}_B^1}{\sqrt{\left(\dot{\Delta}_T^1\right)^2+\left(\dot{\Delta}_B^1\right)^2}}f^1q_N^1\\ q_{f,T}^1&=-\frac{\dot{\Delta}_T^1}{\sqrt{\left(\dot{\Delta}_T^1\right)^2+\left(\dot{\Delta}_B^1\right)^2}}f^1q_N^1\end{aligned} \tag{27}$$

For layer 2:

$$\begin{aligned}q_{f,B}^2&=-\frac{\dot{\delta}_B^2}{\sqrt{\left(\dot{\delta}_T^2\right)^2+\left(\dot{\delta}_B^2\right)^2}}f^2q_N^2\\ q_{f,T}^2&=-\frac{\dot{\delta}_T^2}{\sqrt{\left(\dot{\delta}_T^2\right)^2+\left(\dot{\delta}_B^2\right)^2}}f^2q_N^2\end{aligned} \tag{28}$$

Where, f^i is the friction coefficient on the lower interface of the ith helical layer, q_N^i is the normal force for the ith helical layer (per unit length of a helix) which is the contact pressure, and $\dot{\Delta}_B^1$, $\dot{\Delta}_T^1$ and $\dot{\delta}_B^2$, $\dot{\delta}_T^2$ can be written as

$$\dot{\Delta}_B^1 = \frac{\partial \Delta_B^1}{\partial \varepsilon}, \dot{\Delta}_T^1 = \frac{\partial \Delta_T^1}{\partial \varepsilon}$$
$$\dot{\delta}_B^2 = \frac{\partial \delta_B^2}{\partial \varepsilon}, \dot{\delta}_T^2 = \frac{\partial \delta_T^2}{\partial \varepsilon} \tag{29}$$

The derivative form denotes sliding velocity with respect to bending curvature (ε=r/R=$r\cdot\kappa$), and this approach of friction on helical layers was followed by Leroy and Estrier's model [17].

3. Quasi-linear method

Since all the equations are obtained by previous demonstration, this mechanical problem can be solved mathematically. Assuming a simplified manner in which distributed moments are neglected, the relation between component distributed loads p_T^i, p_B^i in Eq. (14) and component frictional forces $q_{f,T}^i$, $q_{f,B}^i$ for two helical layers (i=1,2) may be represented by the following matrix form,

$$\begin{bmatrix} p_T^i \\ p_B^i \end{bmatrix} = \begin{bmatrix} q_{f,T}^i \\ q_{f,B}^i \end{bmatrix} - \begin{bmatrix} \cos\overline{\alpha} & -\sin\overline{\alpha} \\ \sin\overline{\alpha} & \cos\overline{\alpha} \end{bmatrix} \begin{bmatrix} q_{f,T}^{i+1} \\ q_{f,B}^{i+1} \end{bmatrix} \tag{30}$$

and the relation between component distributed loads p_N^i and the normal force q_N^i for two helical layers (i=1,2) is given by

$$p_N^i = q_N^{i+1} - q_N^i \tag{31}$$

by substituting Eqs. (30) and (31) into Eq. (14), the final equilibrium equations can be validated and shown as

$$\frac{dF_T^i}{ds} - F_B^i \kappa_g^i - F_N^i \kappa_n^i + q_{f,T}^i - q_{f,T}^{i+1}\cos\overline{\alpha} + q_{f,B}^{i+1}\sin\overline{\alpha} = 0 \tag{32}$$

$$\frac{dF_N^i}{ds} + F_T^i \kappa_n^i + F_B^i \tau_g^i - q_N^i + q_N^{i+1} = 0 \tag{33}$$

$$\frac{dF_B^i}{ds} + F_T^i \kappa_g^i - F_N^i \tau_g + q_{f,B}^i - q_{f,T}^{i+1}\sin\overline{\alpha} - q_{f,B}^{i+1}\cos\overline{\alpha} = 0 \tag{34}$$

$$\frac{dM_T^i}{ds} - M_B^i \kappa_g^i - M_N^i \kappa_n^i = 0 \tag{35}$$

$$\frac{dM_N^i}{ds} + M_T^i \kappa_n^i + M_B^i \tau_g^i - F_B^i = 0 \tag{36}$$

$$\frac{dM_B^i}{ds} + M_T^i \kappa_g^i - M_N^i \tau_g^i + F_N^i = 0 \tag{37}$$

This system of equations applies to both layers 1 and 2 (i=1,2) and note that, for the external layer (i=2), if friction caused by the external sheath is neglected, then

$$q_N^{2+1} = 0, q_{f,T}^{2+1} = 0, q_{f,B}^{2+1} = 0$$

Let θ and the relative curvature ε be the only two changing parameters of all equations which will be given in the final process of calculation, considering the constitutive relations of Eq. (15), F_B and F_N will be derived from (36) and (37). According to Eqs. (21)–(23), the expressions of F_B and F_N will be only controlled by one unknown quantity Δ_B. This leads to the subsequent calculation of the contact pressure q_N in (33) and note that, from Eqs. (15) and (16), it can be shown that F_T is a function of unknown quantity Δ_T. q_N will be controlled both by Δ_B and Δ_T. Finally, by substituting Eqs. (33), (36) and (37) into Eqs. (32) and (34), the final equations to be solved are Eqs. (32) and (34).

It is noted that in the final forms of Eqs. (32) and (34), the unknown quantities are wire slips Δ_B and Δ_T, other terms like r, R and α will be given as constants when calculation begins. For convenience, the parameter s in differential terms can be replaced by θ using Eq. (20). Thus, the two unknown quantities Δ_B and Δ_T will become the functions of parameters θ and ε. By solving Eqs. (32) and (34) for each layer, it will be clearly shown how wire slips Δ_B and Δ_T vary directly with the parameters θ and ε. Finally, all the other unknown quantities like strains, stresses and moments will be derived from the relations with Δ_B and Δ_T.

Since this huge system seems complex and difficult to solve analytically, many authors descend to searching for other solutions like finite element method. With the aid of finite element analysis software, this problem can be solved directly. However, in a mechanical problem, an analytical solution should be prior to be considered. Leroy and Estrier [17] first tried a quasi Newton method to solve a non-linear system, and as is demonstrated before, the process of calculation is not clear, it is uncertain to show which approximation applies to the equations and how efficient this method is to solve the problem.

In the present paper, in order to seek for a unified solution, the final forms of Eqs. (32) and (34) will be simplified to a system of quasi-linear partial differential equations for the purpose of using numerical method and due to quasi-linear method, the solution is more efficient and unified than non-linear method.

3.1. Linearization

By previous demonstration, the final forms of Eqs. (32) and (34) cannot be fully linearized. The present method seeks to keep the linear differential terms only, including first order $d\Delta_B/d\theta$, $d\Delta_T/d\theta$ and second order $d^2\Delta_B/d\theta^2$, $d^2\Delta_T/d\theta^2$ terms and considering all remaining terms corresponding to their linear differential terms as variable parameters. Due to frictional effects, Δ_B and Δ_T will also vary with relative curvature ε, then all the ordinary differential terms will be replaced by partial differential terms.

However, the expressions of these variable parameters are huge and not convenient for calculation. Since these expressions mainly include the constants such as r, R, α and the two changing parameters θ and ε, the method is to replace them by a set of functions using the symbols $\mathscr{A}(\theta,\varepsilon)$, $\mathscr{B}(\theta,\varepsilon)$, $\mathscr{C}(\theta,\varepsilon)$ and $\mathscr{D}(\theta,\varepsilon)$. The calculation then the final four partial differential equations of two layers derived from Eqs. (32) and (34) are

$$\begin{cases} \mathscr{A}_1(\theta,\varepsilon)\cdot\dfrac{\partial^2\Delta_B^1}{\partial\theta^2}+\mathscr{A}_2(\theta,\varepsilon)\cdot\dfrac{\partial^2\Delta_T^1}{\partial\theta^2}+\mathscr{A}_3(\theta,\varepsilon)\cdot\dfrac{\partial\Delta_B^1}{\partial\theta}+\mathscr{A}_4(\theta,\varepsilon)+p_T^1=0 \\ \mathscr{B}_1(\theta,\varepsilon)\cdot\dfrac{\partial^2\Delta_B^2}{\partial\theta^2}+\mathscr{B}_2(\theta,\varepsilon)\cdot\dfrac{\partial^2\Delta_T^2}{\partial\theta^2}+\mathscr{B}_3(\theta,\varepsilon)\cdot\dfrac{\partial\Delta_B^2}{\partial\theta}+\mathscr{B}_4(\theta,\varepsilon)+p_T^2=0 \\ \mathscr{C}_1(\theta,\varepsilon)\cdot\dfrac{\partial^2\Delta_B^1}{\partial\theta^2}+\mathscr{C}_2(\theta,\varepsilon)\cdot\dfrac{\partial\Delta_B^1}{\partial\theta}+\mathscr{C}_3(\theta,\varepsilon)\cdot\dfrac{\partial\Delta_T^1}{\partial\theta}+\mathscr{C}_4(\theta,\varepsilon)+p_B^1=0 \\ \mathscr{D}_1(\theta,\varepsilon)\cdot\dfrac{\partial^2\Delta_B^2}{\partial\theta^2}+\mathscr{D}_2(\theta,\varepsilon)\cdot\dfrac{\partial\Delta_B^2}{\partial\theta}+\mathscr{D}_3(\theta,\varepsilon)\cdot\dfrac{\partial\Delta_T^2}{\partial\theta}+\mathscr{D}_4(\theta,\varepsilon)+p_B^2=0 \end{cases} \tag{38}$$

Where,

$$\begin{aligned} p_T^1 &= q_{f,T}^1 - q_{f,T}^2\cos\overline{\alpha} + q_{f,B}^2\sin\overline{\alpha} \\ p_T^2 &= q_{f,T}^2 \\ p_B^1 &= q_{f,B}^1 - q_{f,T}^2\sin\overline{\alpha} - q_{f,B}^2\cos\overline{\alpha} \\ p_B^2 &= q_{f,B}^2 \end{aligned} \tag{39}$$

The derivation of functions $\mathscr{A}(\theta,\varepsilon)$, $\mathscr{B}(\theta,\varepsilon)$, $\mathscr{C}(\theta,\varepsilon)$ and $\mathscr{D}(\theta,\varepsilon)$ is processed in Maple environment, which is not included here, since the expressions are complicated to present. However, the process of derivation is clear and simple by means of previous demonstration in Eqs. (32) and (34).

Meanwhile, the expressions of $q_{f,B}$ and $q_{f,T}$ are given by Eqs. (27) and (28).

The frictional part in Eq. (38) is still not explicit. The difficulty is that the differential terms in Eqs. (27) and (28) are intricate and hard to use in numerical methods. In order to turn into a quasi-linear differential form, let,

$$\begin{aligned} \Theta_1 &= -f\cdot\frac{q_N^1}{\sqrt{\beta^2+\left(\Delta_T^{1'}\right)^2+\left(\Delta_B^{1'}\right)^2}} \\ \Theta_2 &= -f\cdot\frac{q_N^2}{\sqrt{\beta^2+\left(\delta_T^{2'}\right)^2+\left(\delta_B^{2'}\right)^2}} \end{aligned} \tag{40}$$

Where β is a coefficient employed to avoid numerical problem only when the denominator is zero and then the formulas of $q_{f,T}$,$q_{f,B}$ will be given by substituting Eq. (40) into Eqs. (27)–(28)

$$q^1_{f,T} = \Theta_1 \cdot \frac{\partial \Delta^1_T}{\partial \varepsilon}$$
$$q^1_{f,B} = \Theta_1 \cdot \frac{\partial \Delta^1_B}{\partial \varepsilon} \tag{41}$$

$$q^2_{f,T} = \Theta_2 \cdot \left(\frac{\partial \Delta^2_T}{\partial \varepsilon} - \frac{\partial \Delta^1_B}{\partial \varepsilon} \sin\overline{\alpha} - \frac{\partial \Delta^1_T}{\partial \varepsilon} \cos\overline{\alpha} \right)$$
$$q^2_{f,B} = \Theta_2 \cdot \left(\frac{\partial \Delta^2_B}{\partial \varepsilon} - \frac{\partial \Delta^1_B}{\partial \varepsilon} \cos\overline{\alpha} + \frac{\partial \Delta^1_T}{\partial \varepsilon} \sin\overline{\alpha} \right) \tag{42}$$

Hence, Eq. (38) has become a system of quasi-linear partial differential equations. The quasi-linear terms are $\mathscr{A}$, $\mathscr{B}$, $\mathscr{C}$, $\mathscr{D}$ and Θ respectively corresponding to partial differential terms $\frac{\partial^2 \Delta_B}{\partial \theta^2}$, $\frac{\partial^2 \Delta_T}{\partial \theta^2}$, $\frac{\partial \Delta_B}{\partial \theta}$, $\frac{\partial \Delta_T}{\partial d\theta}$ and $\frac{\partial \Delta_B}{\partial \varepsilon}$, $\frac{\partial \Delta_T}{\partial \varepsilon}$. These four equations are based on Eqs. (32) and (34) for two helical layers. The four unknown quantities are Δ^1_B, Δ^1_T, Δ^2_B and Δ^2_T. If symbols $\mathscr{A}$, $\mathscr{B}$, $\mathscr{C}$, $\mathscr{D}$ and Θ can be confirmed, with one initial condition and two boundary conditions, the partial differential system will be solved numerically.

3.2. Final pending equations by conclusion

It is noted that Eq. (38) is a quasi-linear system which can be summarized in a matrix form. For convenience, let

$$\boldsymbol{\Delta} = \begin{bmatrix} \Delta^1_B & \Delta^1_T & \Delta^2_B & \Delta^2_T \end{bmatrix}^T \tag{43}$$

Thus, Eq. (38) will develop into a unified formula, which can be defined as

$$\boldsymbol{A} \cdot \frac{\partial^2 \boldsymbol{\Delta}}{\partial \theta^2} + \boldsymbol{B} \cdot \frac{\partial \boldsymbol{\Delta}}{\partial \theta} + \boldsymbol{C} + \boldsymbol{D} \cdot \frac{\partial \boldsymbol{\Delta}}{\partial \varepsilon} = 0 \tag{44}$$

Where,

$$\boldsymbol{A} = \begin{bmatrix} \mathscr{A}_1 & \mathscr{A}_2 & 0 & 0 \\ 0 & 0 & \mathscr{B}_1 & \mathscr{B}_2 \\ \mathscr{C}_1 & 0 & 0 & 0 \\ 0 & 0 & \mathscr{D}_1 & 0 \end{bmatrix} \tag{45}$$

$$\boldsymbol{B} = \begin{bmatrix} \mathscr{A}_3 & 0 & 0 & 0 \\ 0 & 0 & \mathscr{B}_3 & 0 \\ \mathscr{C}_2 & \mathscr{C}_3 & 0 & 0 \\ 0 & 0 & \mathscr{D}_2 & \mathscr{D}_3 \end{bmatrix} \tag{46}$$

$$\boldsymbol{C} = \begin{bmatrix} \mathscr{A}_4 \\ \mathscr{B}_4 \\ \mathscr{C}_4 \\ \mathscr{D}_4 \end{bmatrix} \tag{47}$$

$$\boldsymbol{D} = \begin{bmatrix} 0 & \Theta_1 + \Theta_2 & \Theta_2 \sin\overline{\alpha} & -\Theta_2 \cos\overline{\alpha} \\ -\Theta_2 \sin\overline{\alpha} & -\Theta_2 \cos\overline{\alpha} & 0 & \Theta_2 \\ \Theta_1 + \Theta_2 & 0 & -\Theta_2 \cos\overline{\alpha} & -\Theta_2 \sin\overline{\alpha} \\ -\Theta_2 \cos\overline{\alpha} & \Theta_2 \sin\overline{\alpha} & \Theta_2 & 0 \end{bmatrix} \tag{48}$$

Eq. (44) is the final pending equation which is a common linear partial differential form in mathematical model and it is difficult to find a general solution. However, plenty of numerical solutions can be applied to solving this problem. In order to demonstrate the solution, two key points have to be considered. The first is to apply a proper numerical form for Eq. (44). The form should be conditional convergence which can ensure the accuracy of results. The second is to determine the value of coefficients $\boldsymbol{A}$, $\boldsymbol{B}$, $\boldsymbol{C}$ and $\boldsymbol{D}$. The calculation of these coefficients is of vital importance and will have substantial influence on the stability of Eq. (44).

3.3. Numerical solution

Place a grid on the definition domain $\mathbb{R}^2$ through the points with coordinates $(\theta_j, \varepsilon_n)$, where

$$\begin{array}{l}\theta_j=(j-1)\Delta\theta,\quad j=1,2,\ldots,J,\alpha>0\\ \theta_j=2\pi-(j-1)\Delta\theta,j=1,2,\ldots,J,\alpha<0\\ \varepsilon_n=(n-1)\Delta\varepsilon,\quad n=1,2,\ldots,N,\alpha>0\end{array}\tag{49}$$

Applying finite difference method, the discretized form for differential terms is the following approximation:

$$\frac{\partial^2\boldsymbol{\Delta}(\theta,\varepsilon)}{\partial\theta^2}=\frac{\boldsymbol{\Delta}_{\theta+1,\varepsilon}-2\boldsymbol{\Delta}_{\theta,\varepsilon}+\boldsymbol{\Delta}_{\theta-1,\varepsilon}}{\Delta\theta^2}\tag{50}$$

$$\frac{\partial\boldsymbol{\Delta}(\theta,\varepsilon)}{\partial\theta}=\frac{\boldsymbol{\Delta}_{\theta+1,\varepsilon}-\boldsymbol{\Delta}_{\theta-1,\varepsilon}}{2\Delta\theta}\tag{51}$$

$$\dot{\boldsymbol{\Delta}}=\frac{\partial\boldsymbol{\Delta}}{\partial\varepsilon}=\frac{\boldsymbol{\Delta}_{\theta,\varepsilon}-\boldsymbol{\Delta}_{\theta,\varepsilon-1}}{\Delta\varepsilon}\tag{52}$$

The finite difference form of first order for terms of θ and φ are centered-difference and backward-difference respectively, which are chosen as a guarantee to make the numerical system stable when the rate of step sizes is determined properly.

Moreover, in the formulas of coefficients $\boldsymbol{A}$, $\boldsymbol{B}$, $\boldsymbol{C}$ and $\boldsymbol{D}$, these first and second derivatives also exist, which cannot be calculated in each iterative processing. The quasi-linear solution is obtained, assuming these values are null in the first iterative step, then attempting to use the previous step's formulas by substituting the step number $\varepsilon-1$ into Eqs. (50)–(52) to replace current step's formulas, therefore all the coefficients will develop into known constants in each iterative step. The final finite difference formula derived by Eq. (44) will be given by

$$\boldsymbol{E}_{j,n}\cdot\boldsymbol{\Delta}_{j+1,n}+\boldsymbol{F}_{j,n}\cdot\boldsymbol{\Delta}_{j,n}+\boldsymbol{G}_{j,n}\cdot\boldsymbol{\Delta}_{j-1,n}+\boldsymbol{C}_{j,n}=\boldsymbol{H}_{j,n}\cdot\boldsymbol{\Delta}_{j,n-1}\tag{53}$$

Where,

$$\begin{aligned}\boldsymbol{E}_{j,n}&=\frac{\boldsymbol{A}(\theta=\theta_j,\varepsilon=\varepsilon_n)}{\Delta\theta^2}+\frac{\boldsymbol{B}(\theta=\theta_j,\varepsilon=\varepsilon_n)}{2\Delta\theta}\\ \boldsymbol{F}_{j,n}&=-2\frac{\boldsymbol{A}(\theta=\theta_j,\varepsilon=\varepsilon_n)}{\Delta\theta^2}+\frac{\boldsymbol{D}(\theta=\theta_j,\varepsilon=\varepsilon_n)}{\Delta\varepsilon}\\ \boldsymbol{G}_{j,n}&=\frac{\boldsymbol{A}(\theta=\theta_j,\varepsilon=\varepsilon_n)}{\Delta\theta^2}-\frac{\boldsymbol{B}(\theta=\theta_j,\varepsilon=\varepsilon_n)}{2\Delta\theta}\\ \boldsymbol{H}_{j,n}&=-\frac{\boldsymbol{D}(\theta=\theta_j,\varepsilon=\varepsilon_n)}{\Delta\varepsilon}\end{aligned}\tag{54}$$

This formula can be simplified as the following matrix form which will be calculated in programming by iteration as the final expression.

$$[\boldsymbol{K}][\boldsymbol{\Delta}_n]=[\boldsymbol{L}][\boldsymbol{\Delta}_{n-1}]-[\boldsymbol{M}],\quad(n=2,3,\ldots,N)\tag{55}$$

Where,

$$[\boldsymbol{\Delta}_n]=\begin{bmatrix}\boldsymbol{\Delta}_{2,n} & \boldsymbol{\Delta}_{3,n} & \cdots & \boldsymbol{\Delta}_{J-1,n}\end{bmatrix}^T\tag{56}$$

$$\begin{bmatrix}\\ \boldsymbol{K}\\ \\ \end{bmatrix}=\begin{bmatrix}\boldsymbol{F}_{2,n} & \boldsymbol{E}_{2,n} & & & 0\\ \boldsymbol{G}_{3,n} & \boldsymbol{F}_{3,n} & \boldsymbol{E}_{3,n} & & \\ & \ddots & \ddots & \ddots & \\ & & \boldsymbol{G}_{J-2,n} & \boldsymbol{F}_{J-2,n} & \boldsymbol{E}_{J-2,n}\\ 0 & & & \boldsymbol{G}_{J-1,n} & \boldsymbol{F}_{J-1,n}\end{bmatrix}\tag{57}$$

$$\begin{bmatrix}\\ \boldsymbol{L}\\ \\ \end{bmatrix}=\begin{bmatrix}\boldsymbol{H}_{2,n} & & \cdots & & 0\\ & \boldsymbol{H}_{3,n} & & & \\ \vdots & & \ddots & & \vdots\\ & & & \boldsymbol{H}_{J-2,n} & \\ 0 & & \cdots & & \boldsymbol{H}_{J-1,n}\end{bmatrix}\tag{58}$$

$$\begin{bmatrix} \\ \boldsymbol{M} \\ \\ \end{bmatrix} = \begin{bmatrix} \boldsymbol{C}_{2,n} \\ \boldsymbol{C}_{3,n} \\ \vdots \\ \boldsymbol{C}_{J-2,n} \\ \boldsymbol{C}_{J-1,n} \end{bmatrix} + \begin{bmatrix} \boldsymbol{G}_{2,n} \cdot \Delta_{1,n} \\ 0 \\ \vdots \\ 0 \\ \boldsymbol{G}_{J-1,n} \cdot \Delta_{J,n} \end{bmatrix} \tag{59}$$

$[\boldsymbol{\Delta}_1]$ and $\Delta_{1,n}$,$\Delta_{J,n}$ are the initial condition and boundary conditions respectively. For initial condition, $[\boldsymbol{\Delta}_1]$ is null, since the bending behaviour begins with a straight configuration. Geometrical boundary conditions will be applied corresponding to both two ends of armour wires' model, which are null since these points have no deformation.

The solution presented in the paper is suitable for all genres of flexible risers theoretically. Given a set of data, the slips, stresses, forces and moments can be calculated for various cases. To validate this analytical model, a comparison will be processed with the frictionless results obtained by Østergaard et al. [18] and the results including frictional effects by Leroy and Estrier [17].

4. Case studies

4.1. Without frictional effects

If frictional effects are neglected, $\boldsymbol{D}$ will be zero in Eq. (44), the problem will degenerate into the following system of ordinary differential equations

$$\boldsymbol{A} \cdot \frac{\partial^2 \boldsymbol{\Delta}}{\partial \theta^2} + \boldsymbol{B} \cdot \frac{\partial \boldsymbol{\Delta}}{\partial \theta} + \boldsymbol{C} = 0 \tag{60}$$

It is noted that the unknown quantity $\boldsymbol{\Delta}$ is only controlled by parameter θ. With several inputs of relative curvature ε, wire slips $\boldsymbol{\Delta}$ can be solved under various bending situations by two boundary conditions in which the slips corresponding to both two ends of armour wires' model are null.

By means of software Mathematica and function NDSolve, which can find a numerical solution to the ordinary differential equations, this problem can be solved directly without linearizing the differential terms $\boldsymbol{A}$,$\boldsymbol{B}$ and $\boldsymbol{C}$ as previous illustration.

Since Østergaard et al. [18] investigated only one helical layer, to make a comparison, Eq. (60) can be expanded as the following two equations

$$\begin{cases} \mathscr{A}_1 \cdot \dfrac{\partial^2 \Delta_B}{\partial \theta^2} + \mathscr{A}_2 \cdot \dfrac{\partial^2 \Delta_T}{\partial \theta^2} + \mathscr{A}_3 \cdot \dfrac{\partial \Delta_B}{\partial \theta} + \mathscr{A}_4 = 0 \\ \mathscr{C}_1 \cdot \dfrac{\partial^2 \Delta_B}{\partial \theta^2} + \mathscr{C}_2 \cdot \dfrac{\partial \Delta_B}{\partial \theta} + \mathscr{C}_3 \cdot \dfrac{\partial \Delta_T}{\partial \theta} + \mathscr{C}_4 = 0 \end{cases} \tag{61}$$

Input data are as follows

$$A = b \cdot h = 5 \cdot 10\text{mm}^2 = 50\text{mm}^2$$
$$r = 0.2\text{m}, \kappa \rightarrow 0.1\text{m}^{-1}, E = 2 \cdot 10^{11}\text{Pa}$$

The initial helical wire layer angle needs to be calculated by the pitch arc length L_{pitch}=1m defined by Østergaard et al. [18].

$$\alpha = \arctan \frac{2\pi r}{L_{pitch}} = 51.5^\circ$$

Østergaard et al. [18] studied pure bending situation, as well as a wire on a cylindrical surface subjected to tension. However, the value of the load in the axial direction of the cylinder was not given. In the comparison, considering pure bending condition subjected to multiple relative curvature, the results presented in Figs. 5 and 6 are obtained.

It can be observed that both Δ_B and Δ_T have sinusoidal-like shapes versus θ, and while the bending curvature increases from pure bending, the slip Δ_B increases significantly compared to Δ_T. It means helical wires preferably tend to slide at transverse direction rather than tangential direction.

Considering Eqs. (21)–(23), geodesic curvature $\Delta\kappa_g$, normal curvature $\Delta\kappa_n$ and geodesic torsion $\Delta\tau_g$ can be derived by Δ_B and Δ_T. Note that the results of Δ_B and Δ_T are discrete, therefore numerical method is needed to calculate the first-order and second-order derivatives of Δ_B and Δ_T. Fig. 7 presented here enables comparison with Østergaard et al. [18].

Fig. 7 shows that both $\Delta\kappa_n$ and $\Delta\tau_g$ match well with the results calculated in Ref. [18]. The maximum amplitudes of $\Delta\kappa_n$ and $\Delta\tau_g$ are respectively in a range from 0.07 m^{-1} to 0.08 m^{-1}. The precision data comparison will be shown in next part together

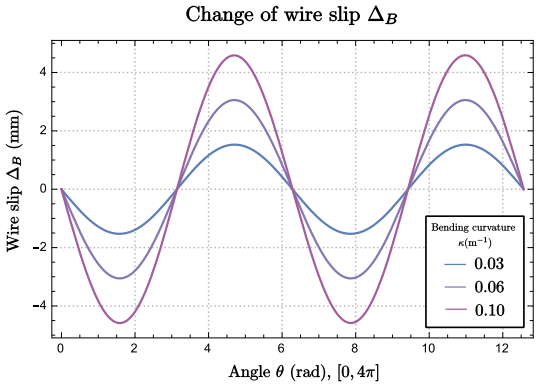

Fig. 5. Change of wire slip Δ_B with no frictional effects.

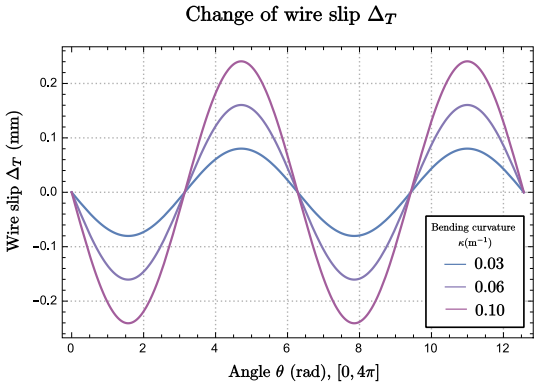

Fig. 6. Change of wire slip Δ_T with no frictional effects.

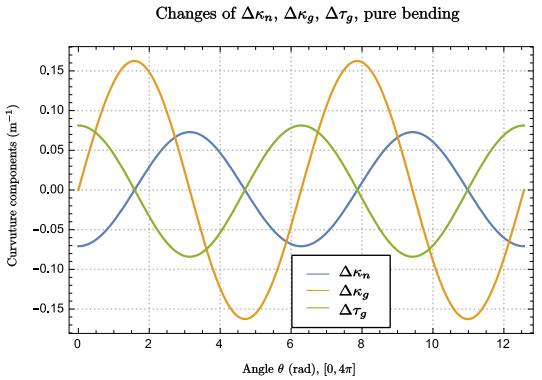

Fig. 7. Changes of wire curvature components, pure bending, $\kappa = 0.1\ \mathrm{m}^{-1}$.

with the frictional case study in tabular form. The analytical method developed in the present paper is reliable and can be a good reference for theoretical discussion of the equilibrium state of one wire on a frictionless toroid.

4.2. With frictional effects

If frictional effects are included, the numerical calculation will be implemented by Eq. (44). The situation is that without frictional effects an armour wire will have certain and only one position corresponding to bending cycles. However, the frictional effects force the armour wires to move further and avoid it returning back to previous position. For this reason, the research on how armour wires move subjected to bending cycles has great and important meaning.

In Ref. [17], the flexible pipe is subjected to twenty repeated cycles of curvature from $1/R$=0 to $1/R$=0.1 m^{-1}, and the following input data were used:

$$E = 2\cdot 10^{11}\text{Pa}, A = b\cdot h = 36\text{mm}^2$$
$$\alpha_1 = -35^\circ, \alpha_2 = 35^\circ, r_1 = 78.3\text{mm}, r_2 = 83.8\text{mm}$$
$$f = 0.15, \text{Cycles} : n = 20$$

Since frictional forces are combined with contact pressure, it is needed to apply load in axial direction to tie up the several layers. The flexible pipes will be subjected to both bending and tension, associated with the practical application. From Ref. [17], load in axial direction of the flexible pipe is transformed into initial tangential forces of armour wires for both layer 1 and layer 2 which are defined as $F^1_{T(ini)}$ and $F^2_{T(ini)}$. The inputs are

$$F^1_{T(ini)} = 7500\text{N}, F^2_{T(ini)} = 6300\text{N}$$

Considering Eqs. (15) and (16), F_T is the tangential force only under pure bending. When it is subjected to bending and tension, the method is to add the values of $F^1_{T(ini)}$ and $F^2_{T(ini)}$ to the first equation of Eq. (15) for both two helical layers which will be the correct and complete values of tangential forces.

In the section, calculation will be processed in the MATLAB programming environment.

Firstly, in order to study the response of helical wires, the displacements along two orthogonal directions will be considered. Displacement Δ_B and Δ_T for two armour layers in half a cycle (from $1/R$=0 to $1/R$=0.1 m^{-1}) are presented in Figs. 8–11. These figures show that both Δ_B and Δ_T have sinusoidal-like shapes versus θ which are the same as the situation with no frictional effects due to periodicity.

Secondly, twenty cycles of bending behaviour are simulated. The main purpose for applying twenty cycles is to observe the changes of the helical wires due to repeated cycles. All geometrical and mechanical quantities hold linear relations with Δ_B and Δ_T by linear expressions from Eqs. (21)–(23). The geodesic curvatures will be chosen to analyse the process in this part, see Figs. 12 and 13.

In differential geometry, the geodesic curvature is a significant quantity which represents the minimum distance. That is, if a curve's geodesic curvature is zero, the curve follows the minimum distance on the surface. In Figs. 12 and 13, the geodesic curvatures are stable after several cycles, located right in the two symmetrical sides of zero geodesic curvature. This stable situation can be a valid reference for fatigue analysis.

Thirdly, Figs. 14 and 15 show tangential stresses along internal and external helical wires only caused by pure bending, from a minimum curvature ($1/R$=0) to a maximum curvature ($1/R$=0.1 m^{-1}), for the first and 20th curvature cycles. Note that, the axial stresses of armour wires are presented in many literature. Compared to the analytical model in Ref. [17], the amplitudes of data are both in a range of 50–60 MPa and 30–40 MPa for layer 1 and 2 respectively. Hence, reliability of quasi-linear method proposed in the paper is certified.

According to Eq. (15), the stress can be deduced by strain γ which has a linear expression with respect to Δ_T in Eq. (16). These figures present that compared with the variations of transverse displacements, changes of tangential displacements during repeated bending are smaller. It means the helical wires are more likely to move transversely and the tangential slips region is stable during repeated cycles of bending.

The fourth part is to make a comparison by investigating the displacement changes along another local frame $\boldsymbol{t}_\theta$ and $\boldsymbol{t}_\varphi$, see Fig. 16. Eq. (24) illustrates the relation between the two kinds of displacements.

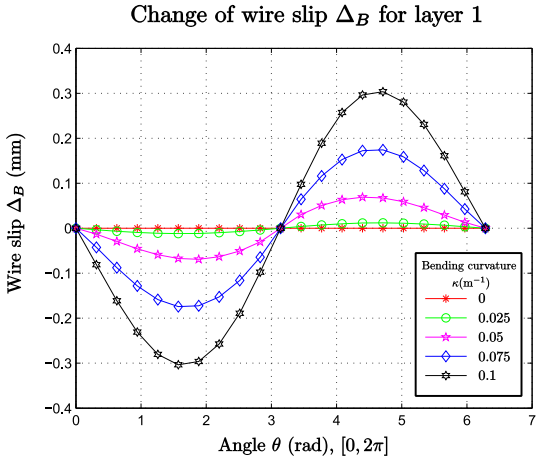

Fig. 8. Change of wire slip Δ^1_B for layer 1.

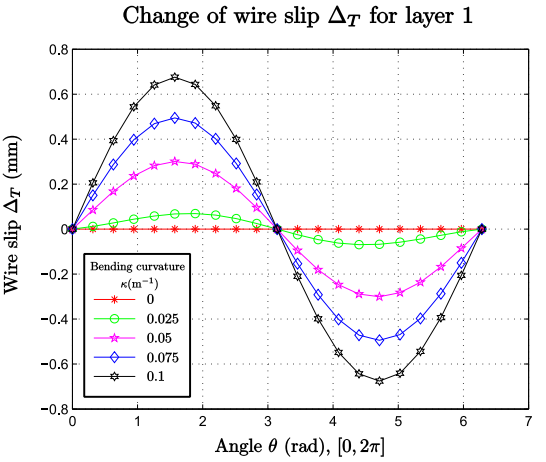

Fig. 9. Change of wire slip Δ_{T}^{1} for layer 1.

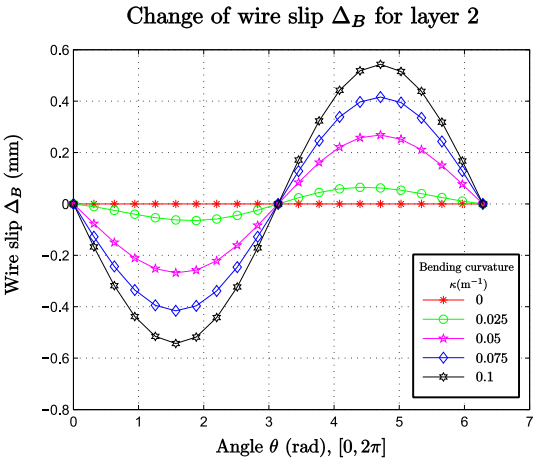

Fig. 10. Change of wire slip Δ_{B}^{2} for layer 2.

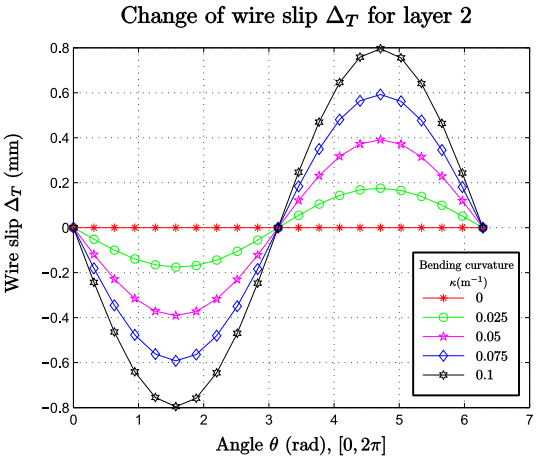

Fig. 11. Change of wire slip Δ_{T}^{2} for layer 2.

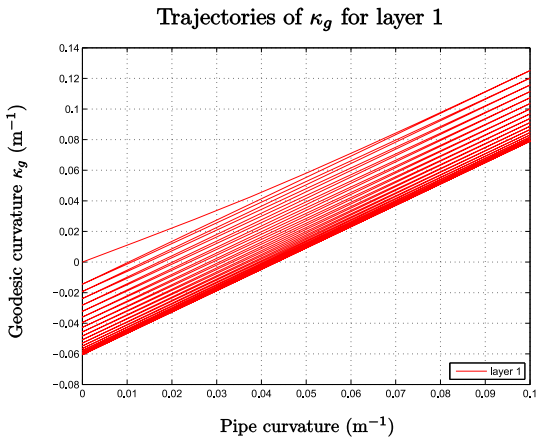

Fig. 12. Change of κ_g, internal layer.

The data are mainly included here in order to ensure the accuracy of the results and all the figures mentioned above match well with Leroy and Estrier [17].

In order to make precise comparison with other analytical model, the adequate data comparison with and without frictional effects is shown in the following Table 1, including the main data of Figs. 7 and 16.

From Table 1, it is clear to figure out the main results between quasi-linear and original solution by Refs. [18] and [17]. The result error is enough small to support feasibility of quasi-linear method. Moreover, compared to nonlinear method, quasi-linear method shows a unified numerical implementation, which can be available for various cases in practical configurations, and nonlinear method is needed to adjust the algorithms for every condition in case of the issue caused by instability.

Furthermore, in order to study some extended situations, different initial layer angles, initial tangential forces and friction coefficients are applied to investigate the changes of slips. The initial tangential forces vary from 7500 N to 9500 N with an increment of 1000 N. The different initial helical layer angles are determined by 35, 45, 55 C$\circ$. Meanwhile, 0.05, 0.10, 0.15 will be chosen as three values of friction coefficients.

In this part, displacement Δ_B in internal layer will be chosen as the typical example to show and represent the results since all displacements exhibit similar motions, see Figs. 17 and 20.

These figures show some reasonable slip changes while applying different initial layer angles, initial tangential forces and friction coefficients. In Figs. 17 and 18, if increasing loading initial forces or increasing the initial layer angle, the slip will decrease. Meanwhile, in Fig. 19, when friction coefficient increases, the friction force will have a tendency to prevent helical wires moving faster and the slips will also decrease. After several repeated cycles, the slips will tend to stabilize and the friction coefficients show little influence on the final stable situation, see Fig. 20.

It is noted that during repeated cycles of bending, the tangential slips region is stable when applying various coefficients, see Figs. 21 and 22. The displacement Δ_T shows similarly incremental situation as for Δ_B in the first cycle. However, after 20 cycles, the slips keep the same value. The situation is similar to the result of axial stresses in Figs. 14 and 15 which has few changes after several cycles.

Considering bent flexible pipe, the slip behaviour is one of the key research objects since the accurate description is not given in recent literature. There are several hypothesis models of armor wires slips such as axial slip model, loxodromic slip model, geodesic slip model and others respectively in different references. In Ref. [17], the presumptive relation of two coordinates (θ, φ) and strain equation provide a link between mechanical quantities and armour layers slips, which can be used to figure out every changing step of two armour layers slips. The unconstrained view is free for investigation. It is non-essential to allow only one prescribed slip direction. The quasi-linear method proposed in this paper also adopts the above mentioned solution for slip behaviour. Results exhibit a clear and profound changes of slips along the local frame ($\boldsymbol{T}$, $\boldsymbol{B}$) for two armour layers, which can be a reliable reference for investigation of armour wires' movement in bending behaviour study compared to other hypothetical slip model. Furthermore, the extended research indicates that some other factors including initial layer angles, initial tangential forces and friction coefficients also have significant influence on the change of slips.

5. Conclusion

In this work the bending behaviour of two helical layers of flexible risers with friction was presented. On basis of geometrical and mechanical models, a system of quasi-linear partial differential equations was established to generate an analytical solution. Numerical implementation was written in detail to formulate a unified method which will have a wide range of applications in bending and fatigue behaviour research of flexible risers theoretically.

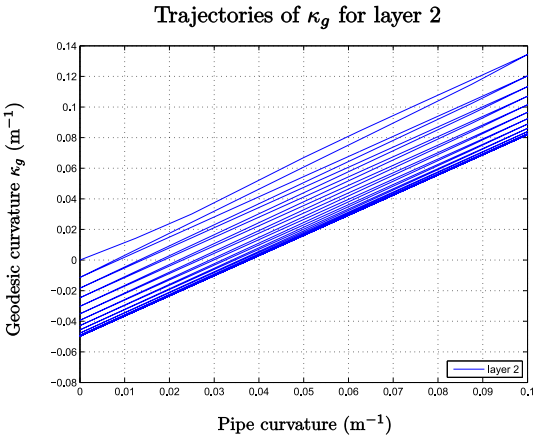

Fig. 13. Change of κ_g, external layer.

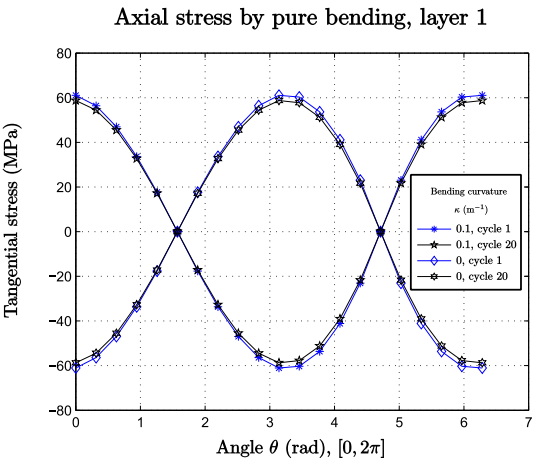

Fig. 14. Axial stress, internal layer.

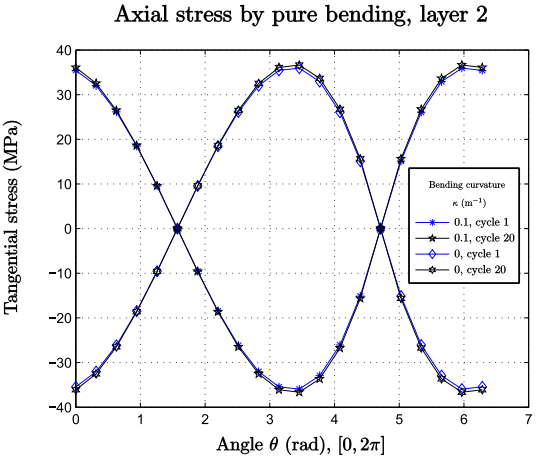

Fig. 15. Axial stress, external layer.

Two case studies have been investigated in the paper, including the theoretical discussions of the equilibrium state of armour wires with and without frictional effects. The calculation in the study shows that the slips corresponding to bending all have sinusoidal-like shapes versus the arc length s or parameter θ and tend to be stable within a range in accordance with

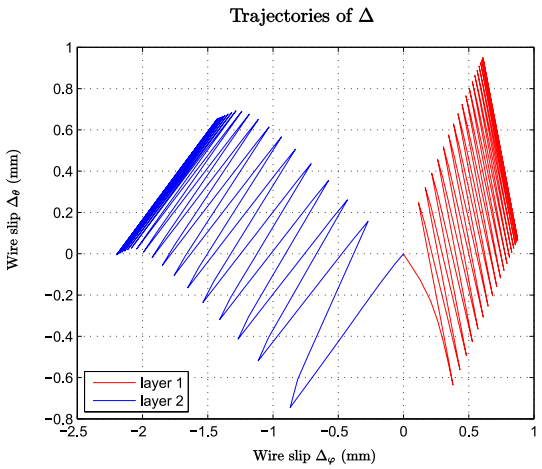

Fig. 16. Trajectories of wire slip Δ_θ and Δ_φ.

Table 1
Inputs of experiment data.

Model	Without friction Amplitudes of curvature (m^{-1})			With friction (Slips along frame ($\boldsymbol{t}_\theta$,$\boldsymbol{t}_\varphi$), (mm))			
				Slip range, 20 cycle, layer 1		Slip range, 20 cycle, layer 2	
	$\Delta\kappa_g$	$\Delta\kappa_n$	$\Delta\tau_g$	Δ_θ	Δ_φ	Δ_θ	Δ_φ
Østergaard et al. [18]	0 ~ 0.05	0 ~ 0.06	0 ~ 0.05	/			
Leroy and Estrier [17]	/			0.10 ~ 0.80	0.60 ~ 0.95	−0.05 ~ 0.40	−2.00 ~ −1.50
Quasi-linear method	0 ~ 0.16	0 ~ 0.07	0 ~ 0.08	0.08 ~ 0.95	0.60 ~ 0.85	0.00 ~ 0.65	−2.20 ~ −1.40

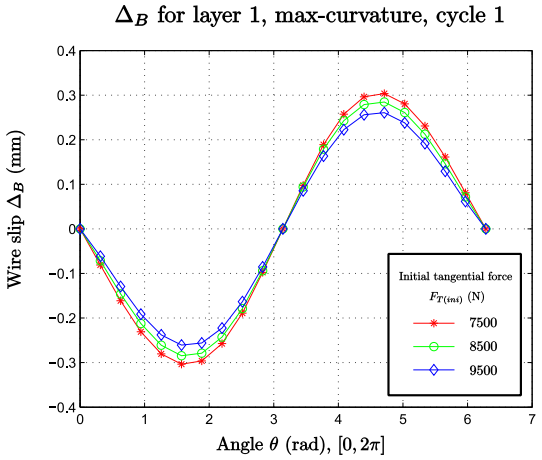

Fig. 17. Change of Δ_B^1, cycle 1.

other analytical results. In addition, various initial layer angles, initial tangential forces and friction coefficients are applied to investigate the change of slips. All the data and results can be a satisfactory reference for future study of bent helical wires.

Although the study presented in this paper found evidence for predicting repeated bending behaviour, from the data collected it was not possible to determine when the slip exactly occurs and point out the direction of slips for both two armour layers. Further studies are therefore necessary to study the principle of slippage and separate the region before and after slip to improve the frictional model. Meanwhile, the quasi-linear method proposed in the paper is apparently sensitive to the initial conditions, and accuracy cannot be certified specifically when simplifying all equations into a quasi-linear system. The disadvantages mentioned above are exactly in need of improvement. Furthermore, the bending problem only includes the contribution from tensile armour layers, the reliable prediction of bending stiffness for multiple layers is needed to be investigated in the future.

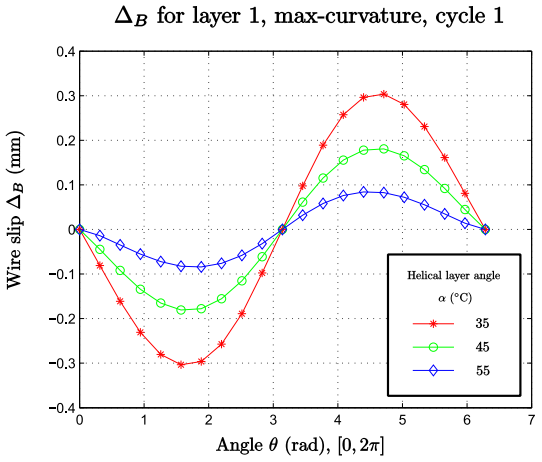

Fig. 18. Change of Δ_B^1, cycle 1.

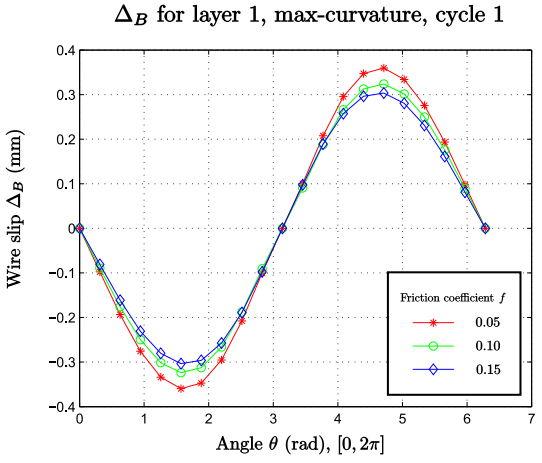

Fig. 19. Change of Δ_B^1, cycle 1.

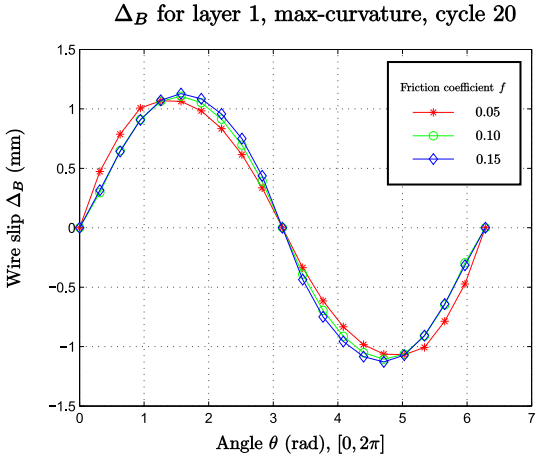

Fig. 20. Change of Δ_B^1, cycle 20.

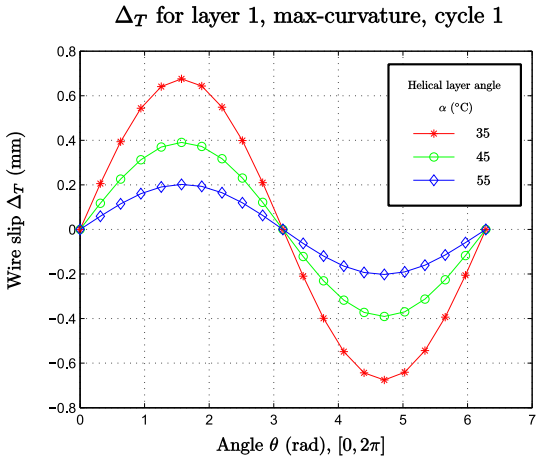

Fig. 21. Change of Δ_t^1, cycle 1.

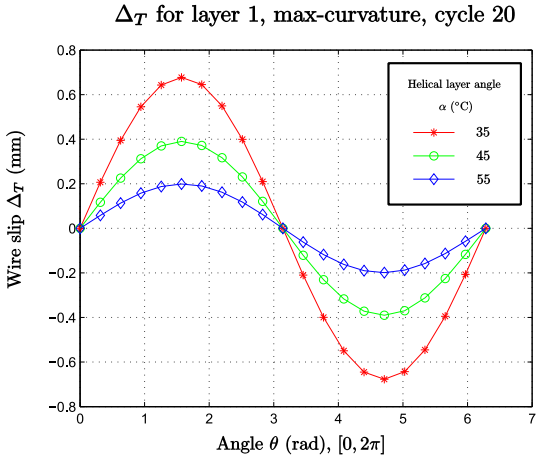

Fig. 22. Change of Δ_t^1, cycle 20.

References

[1] Féret J, Bournazel C. Calculation of stresses and slip in structural layers of unbonded flexible pipes. J Offshore Mech Arct Eng 1987;109(3):263–9.
[2] Out J, von Morgen B. Slippage of helical reinforcing on a bent cylinder. Eng Struct 1997;19(6):507–15.
[3] Witz J, Tan Z. On the flexural structural behaviour of flexible pipes, umbilicals and marine cables. Mar Struct 1992;5(2):229–49.
[4] Sævik S. A finite element model for predicting stresses and slip in flexible pipe armouring tendons. Comput Struct 1993;46(2):219–30.
[5] Sævik S, Bruaseth S. Theoretical and experimental studies of the axisymmetric behaviour of complex umbilical cross-sections. Appl Ocean Res 2005;27(2):97–106.
[6] Sævik S. Theoretical and experimental studies of stresses in flexible pipes. Comput Struct 2011;89(23):2273–91.
[7] Sævik S, Thorsen MJ. Techniques for predicting tensile armour buckling and fatigue in deep water flexible pipes, in: ASME 2012 31st International Conference on Ocean, Offshore and Arctic Engineering. Am Soc Mech Eng 2012:469–82.
[8] Sævik S, Li H. Shear interaction and transverse buckling of tensile armours in flexible pipes, in: ASME 2013 32nd International Conference on Ocean, Offshore and Arctic Engineering. Am Soc Mech Eng 2013. V04AT04A013–V04AT04A013.
[9] Sævik S, Gjøsteen J. Strength analysis modelling of flexible umbilical members for marine structures. J Appl Math 2012;2012:18. http://dx.doi.org/10.1155/2012/985349. Article ID 985349.
[10] Costello GA. Theory of wire rope. Springer Science & Business Media; 1997.
[11] Ramos R, Pesce CP. A consistent analytical model to predict the structural behavior of flexible risers subjected to combined loads. J Offshore Mech Arct Eng 2004;126(2):141–6.
[12] Brack M, Troina LM, de Sousa JRM. Flexible riser resistance against combined axial compression, bending, and torsion in ultra-deep water depths. In: ASME 2005 24th International Conference on Offshore Mechanics and Arctic Engineering. American Society of Mechanical Engineers; 2005. p. 821–9.
[13] Bahtui A, Bahai H, Alfano G. A finite element analysis for unbonded flexible risers under axial tension. In: ASME 2008 27th International Conference on Offshore Mechanics and Arctic Engineering. American Society of Mechanical Engineers; 2008. p. 529–34.
[14] Bahtui A, Bahai H, Alfano G. A finite element analysis for unbonded flexible risers under torsion. J Offshore Mech Arct Eng 2008;130(4):041301.
[15] Féret J, Leroy J, Estrier P. Calculation of stresses and slips in flexible armor layers with layers interaction, Tech. rep. New York, NY (United States): American Society of Mechanical Engineers; 1995.
[16] J. Féret, G. Momplot, reportCaflex-a program for capacity analysis of flexible pipes, Theory Manual, SINTEF Report no.: STF.
[17] Leroy J, Estrier P. Calculation of stresses and slips in helical layers of dynamically bent flexible pipes. Oil Gas Sci Technol 2001;56(6):545–54.

[18] Østergaard NH, Lyckegaard A, Andreasen JH. A method for prediction of the equilibrium state of a long and slender wire on a frictionless toroid applied for analysis of flexible pipe structures. Eng Struct 2012;34:391–9.
[19] Østergaard NH, Lyckegaard A, Andreasen J. Simulation of frictional effects in models for calculation of the equilibrium state of flexible pipe armouring wires in compression and bending. Rakenteiden Mekaniika J Struct Mech 2011;44(3):243–59.
[20] Yue Q, Lu Q, Yan J, Zheng J, Palmer A. Tension behavior prediction of flexible pipelines in shallow water. Ocean Eng 2013;58:201–7.
[21] Tang M, Lu Q, Yan J, Yue Q. Buckling collapse study for the carcass layer of flexible pipes using a strain energy equivalence method. Ocean Eng 2016;111:209–17.
[22] Tang M, Yang C, Yan J, Yue Q. Validity and limitation of analytical models for the bending stress of a helical wire in unbonded flexible pipes. Appl Ocean Res 2015;50:58–68.
[23] Do Carmo MP. Differential geometry of curves and surfaces, vol. 2. Prentice-hall Englewood Cliffs; 1976.
[24] Reissner E. On finite deformations of space-curved beams. Z für Angew Math Phys ZAMP 1981;32(6):734–44.
[25] Ericksen J, Truesdell C. Exact theory of stress and strain in rods and shells. Archive Ration Mech Analysis 1957;1(1):295–323.
[26] Love AEH. A treatise on the mathematical theory of elasticity, vol. 1. Cambridge University Press; 2013.